Time-Resolved Study of the Oxidation of Ethanol by Cerium(IV) Using Combined Quick-XANES, UV−Vis, and Raman Spectroscopies

V. Briois,[†,‡] D. Lützenkirchen-Hecht,*[,§] F. Villain,[†,||] E. Fonda,[‡] S. Belin,[†] B. Griesebock,[§] and R. Frahm[§]

LURE, Centre universitaire Paris-Sud, BP34, F-91898 Orsay Cedex, France, Synchrotron SOLEIL, L'orme des Merisiers, Saint Aubin, BP48, F-91 192 Gif sur Yvette, France, Institut für Materialwissenschaften und Fachbereich C/Physik, Bergische Universität Wuppertal, Gaussst. 20, D-42097 Wuppertal, Germany, and LCIM2, Bât. F. Case 42, UPMC, 4 place Jussieu, F-75252 Paris Cedex 05, France

Received: July 26, 2004; In Final Form: October 7, 2004

Time-resolved X-ray absorption spectroscopy (Quick-XANES) has been combined with UV−vis and Raman spectroscopies to study the in situ reduction of Ce^{4+} to Ce^{3+} in ethanolic solution with a time resolution of ca. 4−5 s. For this purpose, a cam-driven oscillating double-crystal monochromator with a channel-cut crystal was combined with two spectrometers for UV−vis and Raman spectroscopies in a specialized cell which allows one to fit the optical pathways for all three spectroscopies individually. The results show that high-quality results can be obtained simultaneously, thus giving a detailed insight into the mechanisms of the investigated chemical reaction. The continuous release of nitrate and ethanol ligands from the initial Ce^{4+} into the solution finally leads to a trivalent cerium species which is only coordinated with water molecules after about 1800 s of reaction time.

1. Introduction

The use of complementary techniques in materials science is well-established for obtaining a deep structural description of complex materials. On one hand, the combination of several complementary techniques allows for accessing simultaneously different kinds of information for the same material. Such an approach offers great advantages with respect to separate experiments, to rid oneself of errors due to differences in sample environment, thermal history, aging, temperature, and sample preparation, etc. Researchers are nowadays working to develop analytical tools that can be combined to synchrotron radiation techniques. Pioneering work was done for coupling SAXS (small-angle X-ray scattering) and/or WAXD (wide-angle X-ray diffraction) with other physical techniques, such as laser light scattering,[1] Raman spectroscopy,[1−5] thermal analysis,[2,6−9] Fourier transform infrared spectroscopy,[1,10] and different forms of rheological techniques.[1] Regarding X-ray absorption spectroscopy (XAS), similar combinations are rather scarce[11−14] and not common practice especially for time-resolved studies. Considerable efforts were made during the last 2 years on the D44 beamline of DCI-LURE for combining XAS with robust and flexible instruments for accessing thermodynamic information with differential scanning calorimetry (DSC), electronic information with UV−vis spectroscopy, and vibrational information with Raman spectroscopy. First results were recently presented to illustrate how useful these combined experiments[15] are for the study of static processes in coordination chemistry and catalysis, and the investigation of very slow kinetic reactions in sol−gel chemistry. The performance of the D44 beamline and DCI source (in terms of acquisition time, photon flux available at the sample position, and beam size) limited us to record a few snapshots during the time evolution of the material. The monitoring of events taking place in real time during the synthesis of complex materials or during the exploitation of one of its remarkable properties is crucial for understanding the reaction mechanisms involved during these processes. Such an approach, which is clearly a prerequisite for the rational design of new or more performant materials, requires one to use time-resolved devices and, in the first place, X-ray absorption setups allowing time-resolved experiments such as Quick-XAFS double crystal monochromators[16] or energy-dispersive EXAFS polychromators.[17] Recent developments of the quick-scanning XAFS technique that employ a cam-driven vibrating double crystal monochromator enabled the measurement of full EXAFS spectra of real samples in about 50 ms with the opportunity to measure a reference sample simultaneously.[18,19] This way, it was possible to detect even very small edge shifts and changes of the absorption edge reliably and with a high precision.[20] To illustrate the potential offered by the combination of time-resolved Quick-XANES with UV−vis and Raman spectroscopies, the oxidation of ethanol by ceric ions is a well-suited system which is even suitable as tutorial experiment for students in chemistry.[21] Nevertheless, many details of this reaction on an atomic level are still unknown, which further justifies the present study.

2. Experimental Section

2.1. Data Acquisition. The experiments described here were performed using the synchrotron radiation from the D2 bending magnet of the DCI storage ring (LURE, Orsay, France) operating with 1.85 GeV electrons (injection current of ca. 300 mA, ca. 200 h lifetime). The polychromatic radiation emitted from the bending magnet was monochromatized using a Si(111) channel-cut crystal, which was indirectly cooled via a hollow copper block and a continuous flow of liquid nitrogen.[18] Typical temperatures at the surface of the Si-crystal amount to about

* Corresponding author. E-mail: dirklh@uni-wuppertal.de.
† Centre universitaire Paris-Sud.
‡ Synchrotron SOLEIL.
§ Bergische Universität Wuppertal.
|| LCIM2.

10.1021/jp046691t CCC: $30.25
Published on Web 12/14/2004

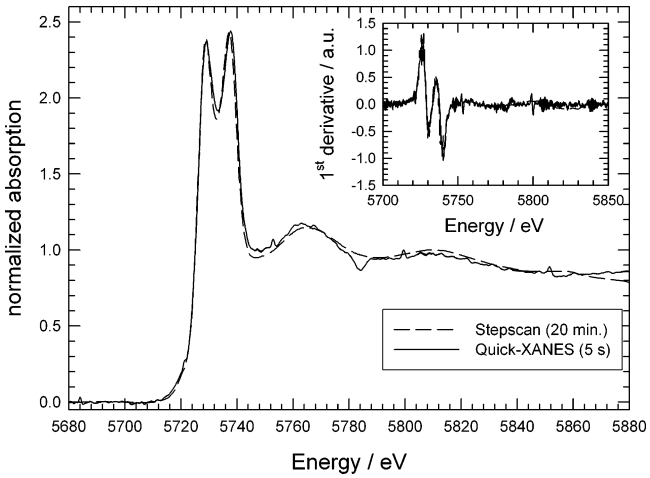

Figure 1. Comparison of XANES scans of the Ce^{4+} initial solution at the Ce L_3-edge (5723 eV). Quick-XANES scan range approximately 200 eV with 0.1 Hz oscillation frequency yielding a spectrum in 5 s with a data sampling rate of 10 kHz; the step scan was measured in 20 min. In the inset, the derivative spectra of both data sets are compared.

110−115 K under the heat load of the X-ray beam. The cooler with the crystal was mounted on a tilt table with two solid-state flexural hinges. A periodic oscillation of this tilt table was achieved by an excenter disk, which is directly mounted on the shaft of a DC-motor. The rotation speed of the motor is controlled by a computer and can be varied from about 0.1 to 40 Hz.[18,19] Several excenter disks with different asymmetries enable one to modify the angular range of the tilt table from about 0.05° to about 1.52°. For the present experiments, a medium cam with an asymmetry of 0.42 mm enables an angular range corresponding to a scan range of about 200 eV at the Ce L_3-edge at 5723 eV. Due to the fact that the attainable time resolution in an X-ray absorption experiment is directly correlated with the available photon flux, the useful oscillation speed was limited to about 1−2 Hz by the flux provided by the DCI bending magnet. The XANES data were obtained in transmission geometry. N_2-filled ionization chambers were used as detectors for the intensity of the incoming and the transmitted radiation. A slit system in front of the first ionization chamber was used to define the horizontal and vertical dimension of the beam to typically 8 mm (h) × 1 mm (v). The current signals from the ionization chambers were converted and amplified by Keithley 428 current-to-voltage amplifiers. Their output signals were directly sampled by a fast A/D converter (4 channels with 16 bit resolution and up to 200 kHz simultaneously) and were stored on a PC computer. Further details of this setup are given elsewhere.[18,19]

Note that time-resolved X-ray absorption results for the same reaction were already reported in the past by Prieto et al.[22] using the same storage ring, DCI. For the latter experiments, the two-crystal monochromator installed on the EXAFS III station was moved continuously from high to low Bragg angle values, allowing one to record each XANES spectrum within 60 s with a dwell time of 24 s, which was the time used by the monochromator to go back to the start position, and by the computer to complete the calculations. The new monochromator used in the current investigation allows for reducing the acquisition time to about 4−5 s per spectrum, without any dwell time between because the rotation of the drive shaft is continuous. As an example, a normalized XANES spectrum of a Ce^{4+}-solution in ethanol measured within 5 s (0.1 Hz oscillation frequency) is compared to a stepscan spectrum of the same solution measured within ca. 20 min in Figure 1. Besides some glitches of the channel-cut monochromator crystal that are visible in the Quick-XANES spectrum at 5750, 5780, 5800, and 5850 eV, both data sets agree quantitatively over the whole data range measured. This can also be seen in the inset of Figure 1, where the first derivatives of both spectra are compared. Thus, it can be concluded that high-quality XANES data of real samples could be measured on a time scale of 5 s at DCI.

UV−vis data were recorded using the Varian Cary 50 dual beam spectrophotometer, working in the 190−1100 nm wavelength range and fitted with a fiber optic coupler. The wavelength range used for the kinetics was between 250 and 750 nm, and the data interval was 1 nm with an average time of 12.5 ms per data point. One UV−vis spectrum every 18 s has been collected. Some characteristics of the Cary 50 apparatus that are favorable for its use in time-resolved studies have been already emphasized.[15]

Raman data were recorded using the RXN1-785 Raman spectrometer from Kaiser Optical Systems, Inc. (KOSI) equipped with a near-IR laser diode working at 785 nm as excitation light and with a CCD detector for providing fast and simultaneous full spectral collection of Raman data from 100 to 3450 cm^{-1}. The laser beam was incident on the sample through a laser probe made of a probehead and an optical fiber for the excitation by the laser. A second optical fiber was used for the collection of the scattered Raman signals. Both fibers were packed in a common sheath of 10 m length. The probehead was equipped with an immersion optic with a long fixed focal length (3 mm) well suited for transparent solutions. The transmitted laser power at the sample position was about 50 mW. A total of 163 spectra with an integration time of 5 s each were acquired. Due to the correction of spurious spikes caused by the detection of cosmic rays for each spectrum and saving of the spectrum, one spectrum is recorded every 13 s in the cycle mode available with the HoloReact software developped by KOSI.

2.2. Materials. All chemicals used were reagent grade. An aqueous solution of 0.1 M ceric ammonium nitrate, $(NH_4)_2Ce(NO_3)_6$, in 2 M HNO_3 was prepared. Absolute ethanol CH_3CH_2OH (0.5 mL, i.e., 8.6 mmol) was added to 25 mL of the ceric-containing solution (2.5 mmol). The resulting solution was mixed in the flask before being transferred into the thermostated cell. The temperature of the thermostated cell was raised from room temperature to 45 °C in about 5 min, and was then maintained at 45 °C for 30 min.

The peculiar design of the thermostated Kel-F cell that is displayed in Figure 2 allows one to record simultaneously X-ray absorption, UV−vis, and Raman data. The optical path for X-ray absorption measurements can be adjusted from a few mm down to ca. 0.2 mm depending on the absorption edge of interest and the concentration of the absorber element. In the present case, the X-ray path length was ∼0.5 mm and two Kapton windows of 12.5 μm were used as X-ray windows. The aperture on the top of the cell allows for use of immersion probes with adjustable optical paths for UV−vis (here 2 mm) and a long focal length for Raman spectroscopy (3 mm).

For convenience purpose, the UV−vis data acquisition has started 4 min before the acquisition of Raman and Quick-XANES data. Both sets of Raman and Quick-XANES data were started and recorded simultaneously. The comparison of data was made using the same time scale, referred to the start of the recording of Raman and Quick-XANES data.

2.3. EXAFS Analysis. The EXAFS data were processed in a conventional manner using the AUTOBK package[23] for the EXAFS extraction and the FeFFiT code for the EXAFS

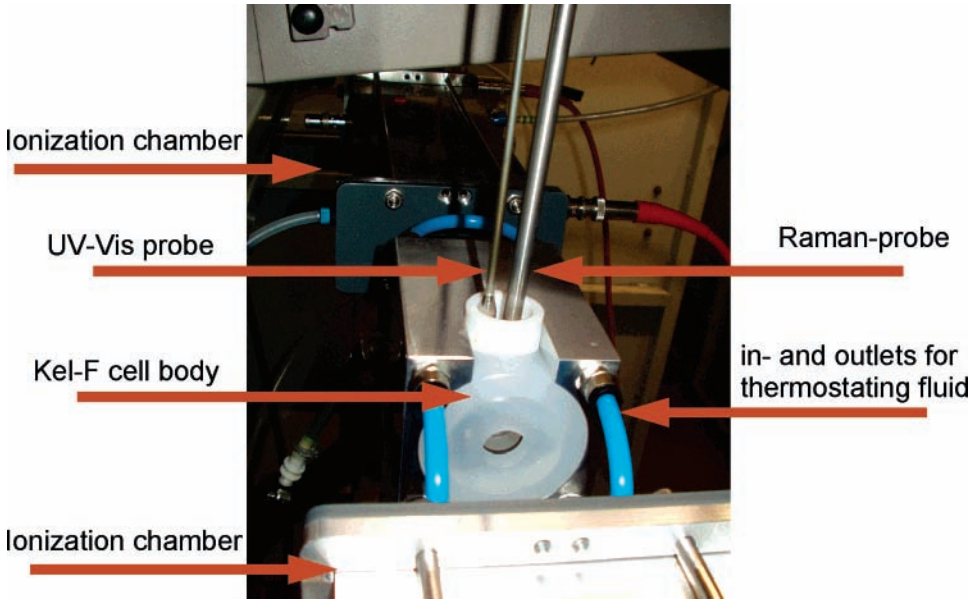

Figure 2. Photograph of the Kel-F thermostated cell located between the two ionization chambers for the collection of the XANES spectra. The UV−vis (on the left) and long-focal length Raman (on the right) immersion probes are in contact with the solution through the aperture at the top of the cell as indicated.

simulation.[24] Phase shifts and amplitude functions were derived from ab initio calculations performed with the FeFF8 code.[25] These functions were first checked on two known solid reference compounds for tetravalent and trivalent cerium: $(NH_4)_2Ce(NO_3)_6$[26] and $Ce_2Mg_3(NO_3)_{12}\cdot 24H_2O$,[27] respectively. The well-known final state configuration interaction which gives rise to a peculiar double-peaked shape of the L_3 edge of tetravalent cerium compounds has been taken into account in the FeFFiT simulations by considering two EXAFS signals which differed only in their k-scale origin by a shift in the threshold energy of 7 eV and in the relative weight of the signal amplitude (i.e., 60% for the EXAFS signal with the origin at the lower energy). Similar procedures were already published for the simulation of the L_3 edge of Ce in CeO_2.[28] The amplitude reduction factor, S_0^2, was first determined for the two reference compounds resulting in $S_0^2 = 0.74$ for $(NH_4)_2Ce(NO_3)_6$ and $S_0^2 = 1.25$ for $Ce_2Mg_3(NO_3)_{12}\cdot 24H_2O$, respectively. These values were then taken as fixed and equal to the so-obtained values related to the oxidation state of cerium. In both cases, least-squares fits were performed in *k*-space or in *R*-space with k^3-weighted fine structure data in the range 2 Å^{-1} < *k* < 9.5 Å^{-1} (1.2 Å < *R* < 5 Å). It should be stressed here that a larger range in *k*-space is not possible due to the onset of the Ce L_2-absorption edge at 6164 eV. It should be mentioned that the simulations include the multiple scattering paths within a nitrate group coordinated in a bidentate fashion to the cerium in both cases. For the species in solution, the path parameters involving the nitrate group are not simulated but just constrained to the distance of the Ce−O distance in the first coordination shell.

3. Results and Discussion

The ceric ion, Ce^{4+}, is a facile oxidant of organic compounds such as ethanol. In that case, ethanol, CH_3CH_2OH, is oxidized into ethanal, $CH_3CH{=}O$, itself susceptible to further oxidation to acetic acid, CH_3COOH. Concomitantly to the oxidation of ethanol, the ceric ion is reduced to the cerous ion, Ce^{3+}. Four molar equivalents of ceric ammonium nitrate are required to stoichiometrically convert one molar equivalent of ethanol to acetic acid. Due to the excess of ethanol in solution as compared to ceric ammonium nitrate for this experiment, it is expected

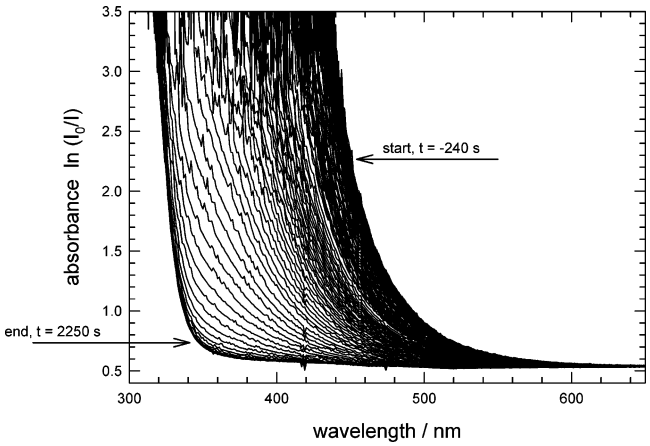

Figure 3. Evolution of UV−vis spectra recorded in the course of the reaction from orange-colored Ce^{4+} to transparent Ce^{3+} as a function of reaction time.

that the ceric ion will be totally reduced at the end of reaction, according to the following reaction:

$$4Ce^{4+} + CH_3CH_2OH \rightarrow 4Ce^{3+} + \text{organic products} \quad (1)$$

The organic products at the end of the reaction will be a mixture of unreacted ethanol, ethanal, and acetic acid.

UV−vis spectroscopy is a well-known technique for monitoring the completeness of reaction 1. Indeed, solutions of ceric salts are yellow or deep orange-red in the presence of ethanol, whereas solutions of cerous salts are colorless. Reaction 1 takes about 24 h at room temperature to be complete. However, the oxido-reduction kinetics can be accelerated by carrying out the reaction at an elevated temperature of 45 °C. In this case, the redox reaction is completed in about 30 min with the thermostated cell used herein.

Figure 3 shows the UV−vis spectra recorded within 35 min involving collection during the heating of solutions from room temperature to 45 °C (∼5 min) and during the isothermal treatment at 45 °C. A continuous color change of the solution with time is observed as Ce^{4+} is converted into Ce^{3+}. After

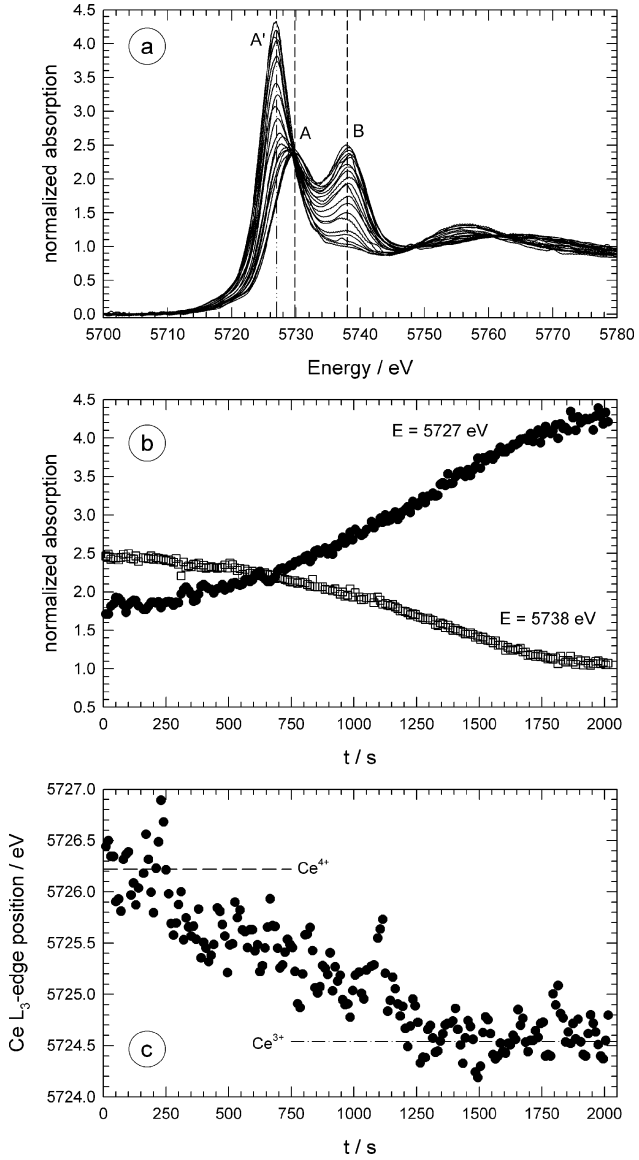

Figure 4. (a) Evolution of the Ce L_3-XANES spectra as a function of time in the course of the reduction of Ce^{4+} to Ce^{3+} in ethanolic solution. Each XANES spectrum was recorded in 5 s. Every 20th spectrum is displayed. (b) Evolution of the normalized absorption intensities at energies corresponding to peak A′ at $E = 5727$ eV and peak B at $E = 5738$ eV as a function of time. (c) Evolution of the edge position determined from the derivative of the XANES spectra. For comparison, the edge positions of Ce^{3+} and Ce^{4+} are indicated.

35 min, the UV−vis spectra do not change any more, suggesting that the reduction of Ce^{4+} is complete.

Simultaneously with the color change, the XANES data displayed in Figure 4a evidence strong modifications in the overall shape of the absorption spectra and the edge energy position. The intensity of the two characteristic peaks (A and B) from Ce^{4+} vanishes with time, while a dominant white line (A′), characteristic of Ce^{3+}, increases in intensity and shifts to lower energy. This can be seen in more detail in Figure 4b and c, where the intensities of the peaks at 5727 eV (peak A′, white line of Ce^{3+}) and 5738 eV (peak B of Ce^{4+}) and the edge position derived from the XANES spectra are displayed as a function of the reaction time, respectively. It should be mentioned here that for $t < 600$ s, an absorption feature corresponding to the white line of Ce^{3+} is not visible in the spectra. Thus, the given values for the absorption at 5727 eV should not be associated with the electronic transition that is responsible for this absorption maximum in the L_3-edge spectrum of Ce^{3+}, and a deconvolution of the experimental data is required to give concentrations of the contributing Ce-species. The existence of isobestic points at about 5730, 5748, and 5763 eV photon energy for the XANES spectra presented in Figure 4a suggests that the evolution of the initial solution toward the final solution does not involve intermediary species. Thus, an intermediate solution should always be a weighted linear combination of the solution containing only the Ce^{4+} species (initial solution) and the solution containing only the Ce^{3+} species (final solution) provided that the reduction is complete. This conclusion is consistent with a principal component analysis (PCA, see, e.g., refs 29 and 30) of the measured XANES spectra, which suggests the presence of only two contributing phases. With PCA, one can determine the minimal number and the type of the model compounds that are necessary to reproduce the measured spectra by means of a linear combination. PCA is equivalent to the methods in linear algebra that are performed to determine the dimensionality of the vector space for the spectra. It is a commonly used tool, for example, for spectroscopic techniques such as mass spectroscopy, infrared spectroscopy, Auger-electron spectroscopy, or UV−vis spectroscopy (see, e.g., refs 29, 30, and 31), and has recently been applied also for the detailed analysis of X-ray absorption spectroscopy data.[32−34] The order in which the standards (reference compounds) are included in the reproduction of the individual spectra is determined by an associated weighting factor. This way, a detailed analysis of XANES and EXAFS is possible. Thus, we tried to fit the experimental spectra to linear combinations of the initial Ce^{4+} and final Ce^{3+} solutions to derive values for the Ce^{4+}/Ce^{3+} composition of the intermediate solutions. The reference spectra for Ce^{4+} and Ce^{3+} were measured in the step-by-step mode at the D44 EXAFS beamline at LURE/DCI. While the Ce^{4+} spectrum was obtained from a freshly prepared ceric solution prepared as described above, the Ce^{3+} solution was measured approximately 1 week after the end of the reduction kinetic of the ceric solution studied by Quick-XANES. The fits were performed for background-subtracted and normalized absorption data in the photon energy range from 5700 to 5800 eV using the WinXas-package.[33] It should be mentioned here that the energy scales of the reference compounds were correlated to each other for the fits, so that only three independent parameters (energy scale, two individual concentrations) were used. Figure 5 displays typical examples of linear combination fits made for two different times in the course of the experiment. In general, the fit quality is good with a residue of less than about 1−2% corresponding to a similar uncertainty in the calculated concentrations.

Figure 6a shows the whole Raman spectrum collected for the first and last spectra of the kinetic reaction, that is, for $t = 0$ s and $t = 2186$ s, respectively. The *Y*-axis was truncated because nitrate being the main strong Raman scatterer of the mixture and its υ_1 vibration located in the 1050−1000 cm^{-1} region otherwise would make the other Raman lines invisible. Several peaks located at 510.3, 718.4, 745.6, 880.1, 915.2, 1048.0, 1455.0, and 1538.0 cm^{-1} are affected during the kinetics, but the most remarkable changes with time are located between 650 and 950 cm^{-1} as shown in Figure 6b. This region contains characteristic vibrations of nitrate ions (the υ_4 vibration for free solvated nitrate ions at 718.4 cm^{-1} and for paired nitrate ions at 745.6 cm^{-1} [35]) and the C−C stretching mode of organic molecules around 850−950 cm^{-1}. These attributions are clearly demonstrated in Figure 6c by considering the Raman spectrum

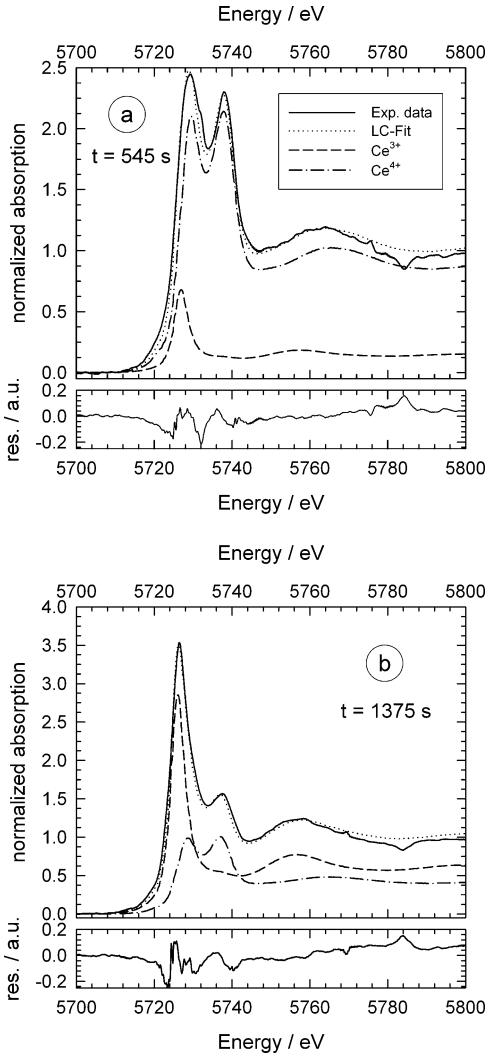

Figure 5. Examples of linear combination made to reproduce the $t = 545$ s (a) and $t = 1375$ s (b) spectra using the step-by-step spectra of the "pure" Ce^{4+} (initial solution) and Ce^{3+} (final solution) species. The difference between the fits and the experimental spectra is indicated in the lower diagrams.

of the ceric ammonium nitrate solution before the addition of ethanol and the Raman spectrum of pure ethanol. For comparison, the first spectrum of the kinetic of ethanol oxidation is also reported. Note that the small peak at 667.5 cm^{-1} is a parasitic peak due to the Kel-F body of the thermostated cell, and thus its intensity does not change with time. Indeed, the Raman bands at 745.6, 1048.0, and 1538.0 cm^{-1} present for the initial solution before the addition of ethanol have been already reported for a 1 M aqueous solution of ceric ammonium nitrate[36] and interpreted as a fingerprint of the coordination of bidentate nitrate groups to Ce^{4+} as suggested by previous XRD results.[37] These bands are assigned to the υ_4, υ_1, and υ_3 vibrations of nitrates, respectively. It is interesting to note that the coordination of nitrate groups to metal affects mainly the υ_4 and υ_3 vibrations, giving rise to a lifting of degeneracy and thus the presence of new components located several cm^{-1} above the bands related to free nitrate[35] (745.6 as compared to 718.4 cm^{-1} for υ_4 and 1538.0 as compared to 1418 cm^{-1} for υ_3). The coordination of nitrate to metal does not lead to a huge lifting of degeneracy for the υ_1 vibration because only asymmetries in the nitrate υ_1 band are evidenced for concentrated or supersaturated nitrate salt solution.[35] In the concentration range investigated in this paper, such an asymmetry is not evident. It

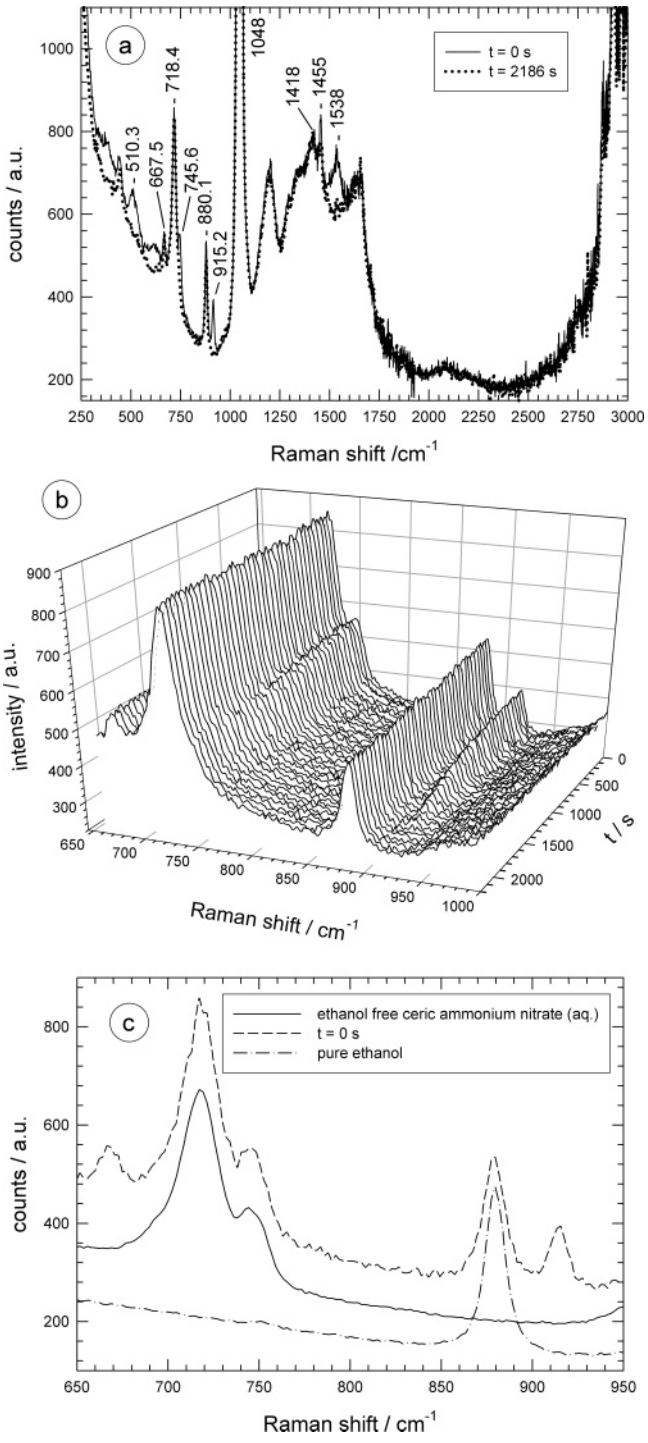

Figure 6. (a) Raman spectra collected at $t = 0$ s (full line) and at $t = 2186$ s (dotted line). (b) Changes of the Raman spectra in the spectral region from 650 to 950 cm^{-1} in the course of the reduction of Ce^{4+} to Ce^{3+} in ethanolic solution. The spectra were recorded every 13 s with an integration time of 5 s. (c) Expanded detail of the Raman spectra recorded for the ceric ammonium nitrate aqueous solution without ethanol (solid line), the spectrum at $t = 0$ s (dashed line), and for pure ethanol (dash−dotted line).

is noteworthy in Figure 6c that pure ethanol species give rise to a single Raman line at 880.1 cm^{-1}; the existence of a second line at higher Raman shift (∼915.2 cm^{-1}) is ascribed to the formation of a cerium(IV)−ethanol complex, noted hereafter "Ce(IV)−EtOH". The formation of this complex with the stoichiometry 1:1 is well known in the literature[38] and serves as a colorimetric method for the detection of alcohol. Indeed,

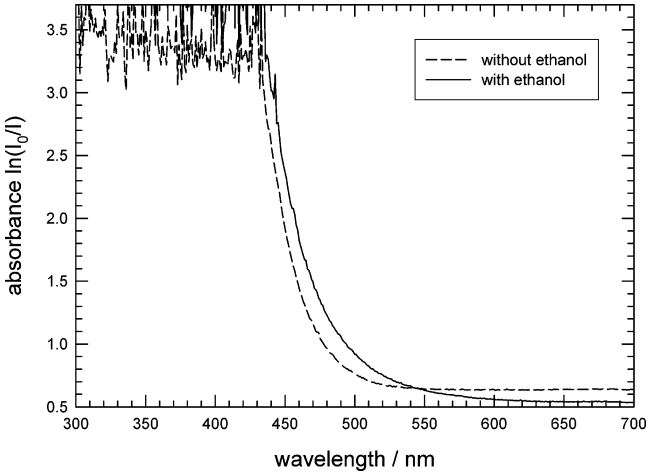

Figure 7. UV−vis evidence of the complexation of Ce^{4+} by EtOH.

when the yellow-orange ceric ammonium solution is mixed with colorless ethanol, an immediate color change to bright red occurs as evidenced in UV−vis spectroscopy (Figure 7). Two remarkable modifications are observed with time in Figure 6b. The shoulder around 745.6 cm^{-1} and the peak at 915.2 cm^{-1} totally disappear upon reduction of cerium, whereas, at first glance, the lines at 718.4 and 880.1 cm^{-1} do not strongly change in intensity. The invariance of these lines is expected because (i) the 2 M HNO_3 media is highly concentrated in free nitrate ions and (ii) the stoichiometry of reaction 1 allows for the estimation of the amount of unreacted ethanol at the end of the redox process ranging from 86% to about 93% if the reaction is totally displaced toward the formation of the acetic acid.

Figure 8 reports the height profile of the characteristic Raman peaks as a function of time. The analysis has been done after subtracting the last spectrum of the kinetic from all other spectra to emphasize small intensity differences. The validity of the procedure has been checked by the absence of the signal at 667.5 cm^{-1}, indicating that the parasitic peak due to the Kel-F body of the cell has been correctly removed after subtraction. The covariance of peaks at 510.3, 745.6, 915.2, and 1538.0 cm^{-1} is displayed in Figure 8a. A scaling factor applied to the peaks at 510.3, 915.2, and 1538.0 cm^{-1} shows clearly the same time evolution for the four considered peaks. The intensity decrease of the shoulder around 745.6 cm^{-1} and of the peak at 915.2 cm^{-1} evidences a change of the Ce^{4+} coordination sphere upon reduction of cerium: a breaking of the bonds between the ceric ion and nitrate ligands as well as between the ceric ion and ethanol molecule occurs. Note that the Raman peak located at 510.3 cm^{-1} is only observed after the addition of ethanol, and then its time evolution allows us to relate this peak to the formation of the Ce(IV)−EtOH complex. Figure 8b reports the covariance of the peaks located at 880.1 cm^{-1} (free ethanol) and at 718.4 and 1048.0 cm^{-1} (free nitrate). As expected, the line at 880.1 cm^{-1} displays a faint decrease in intensity associated to the oxidation of ethanol. Yet its evolution with time is different from that reported in Figure 8a due to the fact that competitive processes occur upon reaction 1. The concentration of ethanol decreases due to its oxidation, but concomitantly a release of ethanol in solution occurs from the decomposition of the Ce(IV)−EtOH complex upon reduction of Ce^{4+}. Similarly, the time evolution of the υ_1 vibration mode for free nitrate ions clearly evidences the breaking of the bond between ceric ion and nitrate ligand upon reduction of Ce^{4+} and release of the corresponding nitrate in solution.

Figure 9 reports the reaction extent versus time for the reduction of Ce^{4+} to Ce^{3+} in the presence of an excess of ethanol

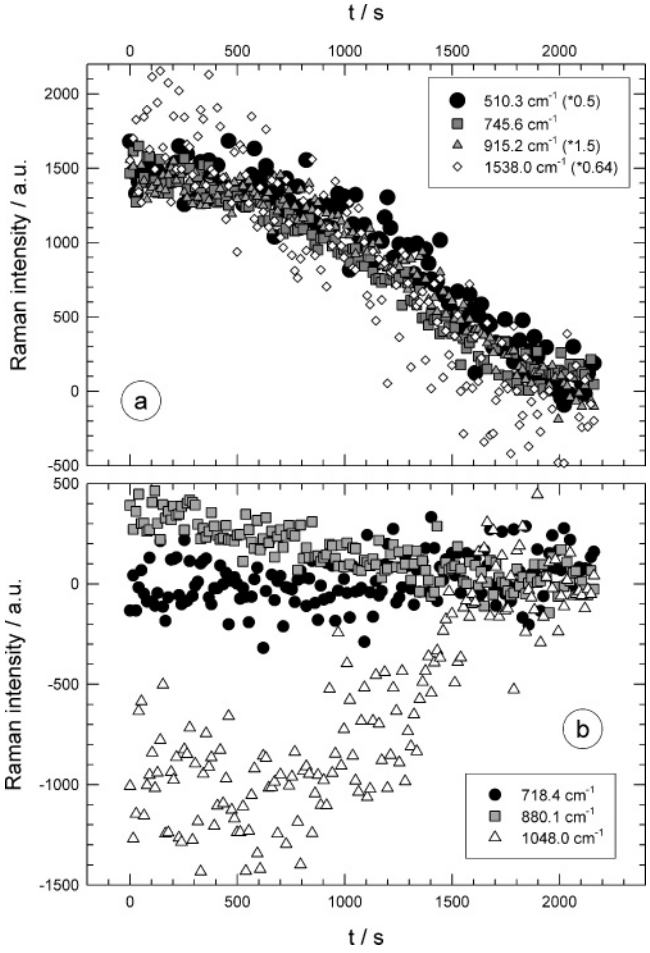

Figure 8. Relative height profile of the Raman peaks located at (a) 510.3, 745.6, 915.2, and 1538 cm^{-1} and (b) 880.1, 718.4, and 1048.0 cm^{-1}. The last raw spectrum of the kinetic has been subtracted from all other raw data, and the scaling factors are indicated for each Raman peak if necessary.

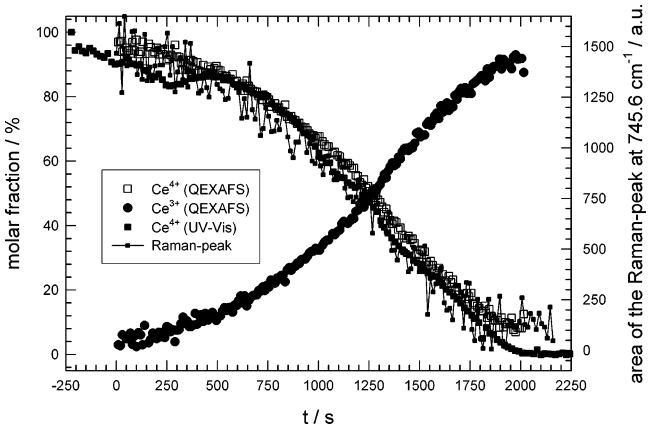

Figure 9. Reaction extent versus time for the reduction of Ce^{4+} in Ce^{3+} in the presence of an excess of ethanol as determined by UV−vis spectroscopy, Raman spectroscopy, and XANES spectroscopy using linear combinations as those shown in Figure 5. For UV−vis, the fraction of Ce^{4+} in solution is reported, while for the Raman data, the area of the peak at 745.6 cm^{-1} is displayed.

as determined by UV−vis spectroscopy, XANES, and Raman spectroscopy. Because only the Ce^{4+} species in reaction 1 is colored, the measured UV−vis absorption is directly related to the Ce^{4+} concentration. To extract quantitative information, the last spectrum of the kinetic was used as a blank spectrum. The agreement between the fraction of Ce^{4+} determined by UV−

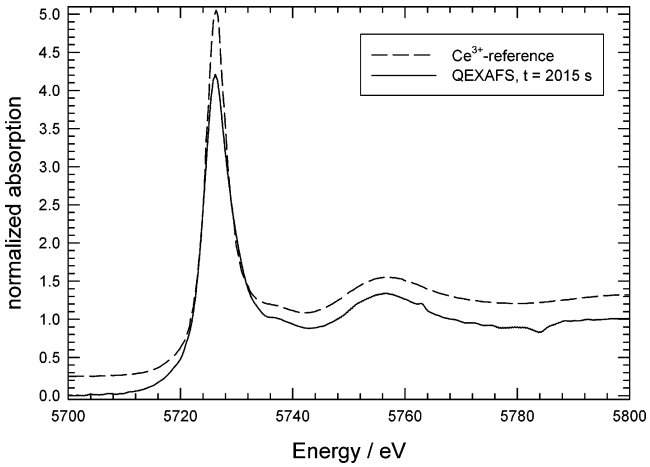

Figure 10. Comparison of Quick-XANES data measured at the end of the kinetic reaction from Ce^{4+} to Ce^{3+} in ethanolic solution (t = 2015 s, full line) and a step-scan spectrum measured 5 days after the initiation of the kinetic reaction (dashed line). The step-scan spectrum is shifted vertically by 0.25 units for clarity.

vis and XANES data is fairly good within 5% of accuracy for kinetic time < 1700 s. At the end of the kinetic (t > 1700 s), the difference between the molecular Ce^{4+} fractions determined by UV−vis and by XANES slightly increases up to 8−9%. A possible explanation for accounting this difference could arise from the fact that the "pure" Ce^{4+} and Ce^{3+} solutions, recorded using the step-by-step setup at beamline D44, and used as principal components of the linear combinations for fitting the XANES data, are not exactly representative of the "pure" Ce^{4+} and Ce^{3+} species in the presence during the kinetic. In particular, it is extremely important to record the first XANES spectrum as fast as possible after the mixture of the aqueous ammonium ceric nitrate solution to the ethanol solution and with an acquisition time as short as possible, because the reduction of Ce^{4+} occurs even at room temperature, although with a longer decay time. While the acquisition time is strongly reduced using the quick-EXAFS monochromator (5 s), a time of ∼20 min is necessary to complete the step-by step XANES acquisition due to the individual monochromator movements in the whole energy range. In addition, there are additional changes of the Ce L_3-absorption spectra of the reduced ceric solution on a time scale of several days as can be seen in Figure 10, where one of the last Quick-XANES spectra measured during the course of the kinetic reaction (t = 2015 s) is compared to the step-scan spectrum measured 1 week after the kinetic has been initiated. While all features in the spectral range displayed are identical for both spectra with respect to their energy and half-width in the pre- and postedge region, obviously the intensity of the Ce^{3+} white line at 5727 eV is more intense in the step-scan spectrum with a value of about 4.80 as compared to about 4.20 at t = 2015 s. Even taking into account the scatter distribution of the derived white line intensities at the end of the kinetic (see Figure 4b), the obtained values are always smaller as compared to that of the Ce^{3+} step-scan spectrum measured several days after the collection of the Quick-XANES data. This finding agrees qualitatively with the analysis of the absorption edge positions in Figure 4c, where the exact absorption edge position of the Ce^{3+} reference (i.e., the Ce^{3+} solution measured in the step-scan mode, E = 5724.54 eV) is not fully reproduced in the course of the reaction kinetics, where a mean value of ca. 5724.62 ± 0.17 eV was derived from the XANES spectra measured between t = 1700 s and t = 2015 s.

The observed deviations in the measured Ce^{3+}-contributions by UV−vis and XANES may also result from the fact that the

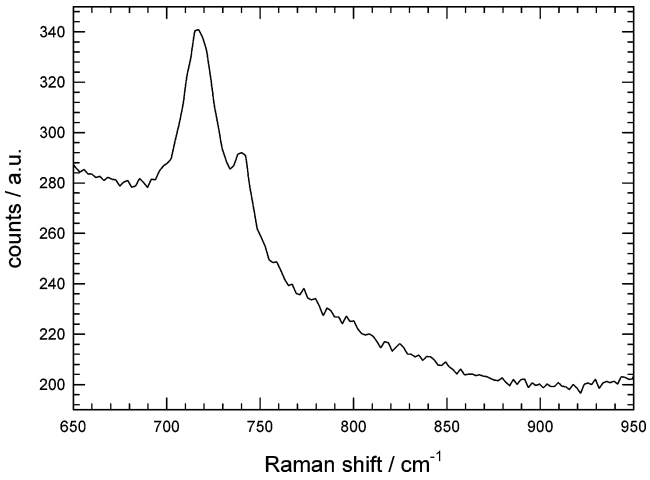

Figure 11. Raman spectrum of a cerous aqueous solution prepared from $Ce(NO_3)_3 \cdot 6H_2O$ salt.

UV−vis data were normalized with respect to the last spectrum measured in the course of the reaction (t = 2250 s), assuming that no remaining contributions of Ce^{4+} are present. Evaluation of the XANES data, however, indicates that there are detectable traces (some few %) of Ce^{4+} in the solution. On the other hand, one should generally keep in mind that the results of the XANES-data evaluation are comparable with the errors of the Raman data (see Figure 9); that is, all of the different techniques give very similar quantitative results for the concentrations of Ce^{3+} and Ce^{4+}.

Due to the similar time evolution of the Raman peaks related to the coordination of nitrate and EtOH by cerium, in Figure 9, only the Raman data related to the peak located at 745.6 cm^{-1} are reported. We must first emphasize that the results obtained from the different techniques are all together consistent. Second, it is clearly pointed out that the oxidation of ethanol and the concomitant reduction of Ce^{4+} involve a change of the cerium coordination sphere, which initially contains nitrate and ethanol ligands. A release of these ligands into the solution occurs, and this study suggests that the coordination sphere of the trivalent cerium species is only made of water molecules. Additional Raman data for a cerous aqueous solution prepared from $Ce(NO_3)_3 \cdot 6H_2O$ salt clearly display the characteristic bands of the chelating nitrate ions at 745.6 cm^{-1} as shown in Figure 11.

Because of the limited beamtime available, we were not able to record a set of extended quick-XAFS data for the same kinetic reaction to study more in detail the changes of the atomic short range order around the cerium atom. Yet our time-resolved study clearly shows that only two cerium species are present during the oxidation of ethanol, that is, the Ce(IV)−EtOH complex and the Ce^{3+} species. Thus, a detailed structural analysis of the reaction under investigation reduces to a detailed modeling of these two compounds, and we have therefore recorded step-by-step EXAFS data for these species similar to those used for the Quick-XANES data evaluation (see Figure 5).

In addition, the formation of the Ce(IV)−EtOH complex has also been investigated through the comparison of the EXAFS data obtained for the ceric ammonium nitrate aqueous solution before the addition of ethanol, referred to hereafter as ethanol-free Ce^{4+} solution. The Fourier transforms (FT) for the three solutions are displayed in Figure 12 together with the Fourier transforms of the $(NH_4)_2Ce(NO_3)_6$ and $Ce_2Mg_3(NO_3)_{12} \cdot 24H_2O$ solid references. The first main peak, labeled A, is related to the first oxygen coordination shell around Ce. As deduced from the FeFFit simulations of the $(NH_4)_2Ce(NO_3)_6$ and $Ce_2Mg_3(NO_3)_{12} \cdot 24H_2O$ solid references (also reported in Figure 12),

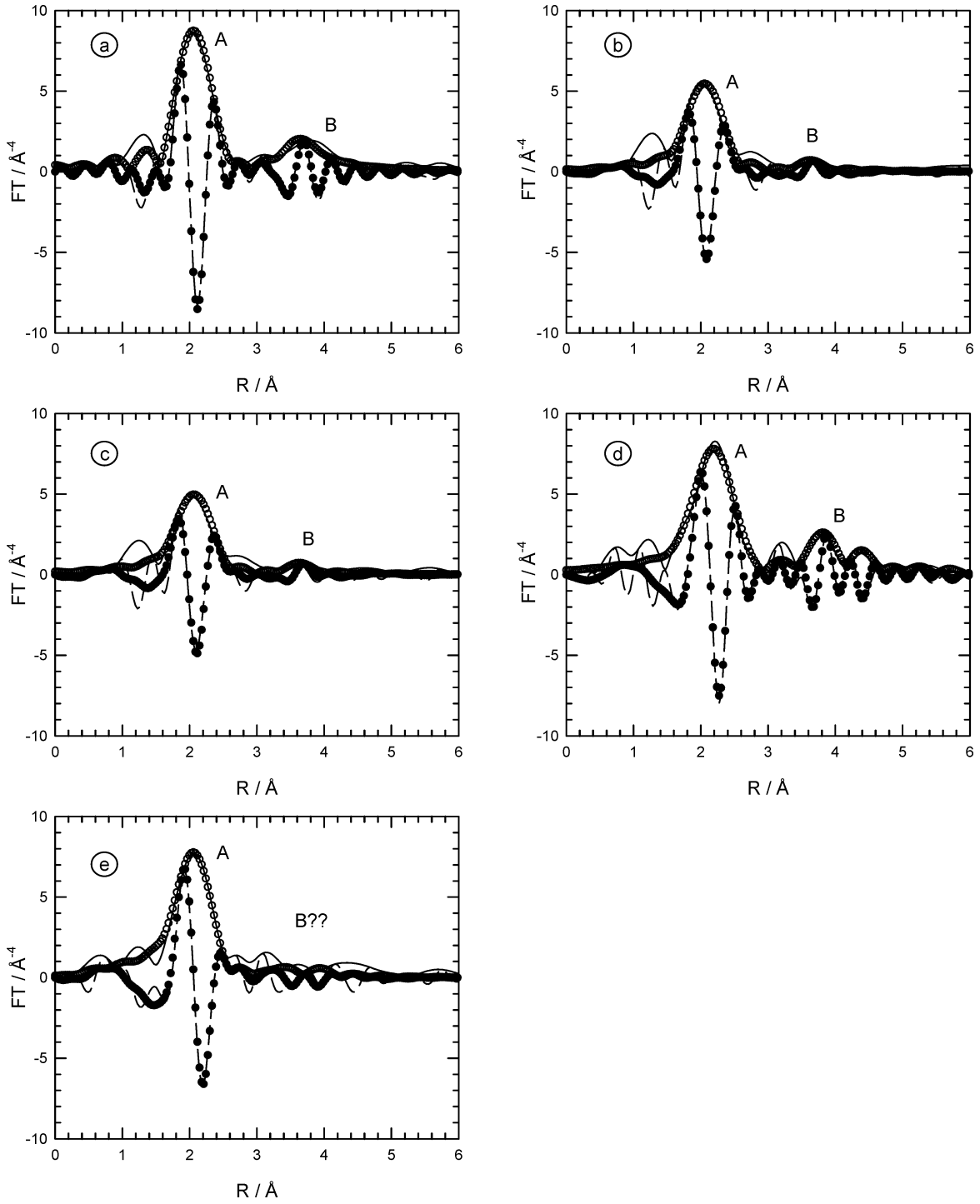

Figure 12. k^3-weighted Fourier transform magnitude and imaginary part of the different EXAFS spectra for (a) $(NH_4)_2Ce(NO_3)_6$ solid compound, (b) free ethanol ceric solution, (c) Ce(IV)−EtOH complex, (d) $Ce_2Mg_3(NO_3)_{12}\cdot 24H_2O$ solid reference, and (e) final cerous solution. Solid lines indicate the experimental data, while the dotted points show the results of fitting with FeFFit.

the second intense peak, labeled B, is a fingerprint for the coordination of the six bidentate nitrate ligands to the cerium with strong multiple scattering effects along all paths involving the nitrate and the noncoordinating oxygen atoms. The decrease in intensity of this peak for the Ce(IV)−EtOH complex and for the ethanol-free Ce^{4+} solution indicates either a change of the chelating behavior of nitrate from bidentate to monodentate nitrate ions or/and a decrease of the number of nitrate ions coordinated to the cerium atom.

From our Raman data, we concluded that the ceric ion is coordinated mainly by bidentate groups, in agreement with findings published in the literature.[36] Therefore, we have performed FeFFit simulations to determine the number of bidentate nitrate ions which are coordinated to Ce^{4+} in the two ceric solutions. The so-obtained structural parameters are summarized in Table 1. It should be mentioned here that we have not considered the alkyl chain of the ethanol for the simulations, which can explain the observed differences between the experimental data and the fits in the FT at around 2.8 Å radial distance. Irrespective of the ethanol content, the first coordination shell of tetravalent cerium in both ceric solutions is made of 12 oxygen atoms located in an average distance of 2.50 Å, with four of these oxygen atoms belonging to bidentate nitrate groups. The Ce^{3+} species is also surrounded by 12

TABLE 1: Structural Parameters Obtained by Fitting the Step-by-Step EXAFS Spectra of the Different Solutions and Solid Reference Compounds[a]

	N	R (Å)	σ^2 (10^{-3} Å^2)	E_0 (eV)	residual factor
solid $(NH_4)_2Ce(NO_3)_6$	12.0 O 6 N	2.507 ± 0.009 2.903 ± 0.118	4.6 ± 0.6 31.7 ± 16	2.2	0.022
XRD for $(NH_4)_2Ce(NO_3)_6$[26]	12.0 O 6 N	2.508 ± 0.007 2.946 ± 0.100			
ethanol-free ceric solution	12.0 O 1.9 N ± 2.8	2.490 ± 0.011 2.902	12.1 ± 1.6 22.6 ± 40.1	3.0	0.153
Ce(IV)−EtOH complex in HNO_3 aqueous solution	12.0 O 2.0 N ± 2.7	2.507 ± 0.022 2.922	12.8 ± 4.4 21.0 ± 35.5	3.0	0.164
solid $Ce_2Mg_3(NO_3)_{12}\cdot 24H_2O$	12.0 O 6 N	2.629 ± 0.022 3.130 ± 0.036	12.8 ± 4.4 10.6 ± 5.9	6.3	0.050
XRD for $Ce_2Mg_3(NO_3)_{12}\cdot 24H_2O$[27]	12.0 O 6 N	2.643 ± 0.031 3.066 ± 0.018			
final cerous solution	12.0 O 0.8 N ± 0.9	2.556 ± 0.008 2.957	15.7 ± 1.4 6.5 ± 16.6	6.3	0.082

[a] For comparison, results of XRD experiments are given for $(NH_4)_2Ce(NO_3)_6$ and $Ce_2Mg_3(NO_3)_{12}\cdot 24H_2O$.

oxygen atoms located at a slightly increased average distance of 2.56 Å. However, the Ce−O distance is decreased by 0.08 Å as compared to the $Ce_2Mg_3(NO_3)_{12}\cdot 24(H_2O)$ crystalline solid;[27] the latter is characterized by a coordination shell of 6 bidentate nitrate groups.

Similarly, we tried to introduce nitrate groups for simulating signals recorded for Ce^{3+} species at larger distances than the distance of the first coordination shell (peak B in the FT). However, contrary to the ceric solutions for which a real improvement of the so-obtained fit could be achieved in particular by the reproduction of the second peak B, the presence of one nitrate group (exactly 0.8 with an uncertainty of 0.9) does not physically improve the fit for the cerous solution (Figure 12e). This is totally in agreement with the Raman results where only free solvated nitrate ions are present in the final cerous solution. Note that the shortening of Ce−O distance of 0.08 Å is also in agreement with the loss of nitrate ions in the coordination sphere of trivalent cerium.

This paper presents new results for the clarification of the effect of the nitrate ligand on the formation of the cerium(IV)−alcohol complex. In ref 21, it has been reported that the complex formation for a ceric ammonium nitrate solution is almost inhibited in H_2SO_4 media, whereas Young and Trahanovsky indicated in ref 38 that the formation constant for the cerium(IV)−alcohol complex is lower in the presence of added nitrate but not in the presence of perchlorate. On the other hand, no changes in the absorbance are observed when alcohol is added to ceric ammonium sulfate, and no evidence for the formation of the cerium(IV)−ethanol complex could be obtained from Raman spectroscopy (not shown here). All of these results could falsely suggest that nitrate ions are competing with alcohol molecules for cerium(IV) coordination sites. In fact, it has been proposed in the literature that such a hexanitrato ceric species exists in solution,[37,38] with an alcohol molecule replacing one of the Ce−O bonds and a new Ce−O bond formed to the alcohol. The 12-fold coordination sphere of the Ce(IV)−EtOH complex is then described as made with five bidentate nitrate groups, one monodentate nitrate group, and one alcohol molecule. Our results confirm the 12-fold oxygen coordination sphere of the Ce(IV)−EtOH complex and the ethanol-free ceric ammonium nitrate species in aqueous solution, respectively. Yet the number of nitrate ligands has been refined to only two bidentate groups instead of five. Furthermore, no strong difference neither in the shape of the FT nor in the structural EXAFS parameters (see Table 1) for the Ce(IV)−EtOH complex and for the ethanol-free ceric ammonium nitrate species in aqueous solution has been evidenced, indicating that the formation of the Ce(IV)−EtOH complex occurs by a nucleophilic substitution of water by alcohol. The observed difference in the formation constant of this complex depending on the media (nitrate, perchlorate, or sulfate) should rather result from differences in the complexing ability of these anions and from hydrolysis−condensation processes which compete in the substitution of water by alcohol.[39]

Finally, we must emphasize one of the advantages of the combination of techniques to study kinetics in chemistry or in materials science. The complementarity of information available by the three spectroscopies is very important for unraveling complex kinetic formation pathways, but also for interpreting the different data in detail. In particular, it is well known that the quantitative analysis of the EXAFS part of the X-ray absorption spectrum suffers from two main drawbacks related to the accuracy in the determination of the coordination numbers (typically between 10% and 20%) and to the identification of the different neighbors in a coordination sphere, when their atomic numbers are too close to each other. For example, for the kinetic reaction studied herein, the complementary use of Raman spectroscopy has allowed us to constrain the structural parameters determined from the analysis of EXAFS spectra by introducing nitrate ion contributions for simulating the EXAFS spectrum of the ceric solutions. Without this additional information, our EXAFS analysis for the ceric solution could be open to criticism because the nitrate contribution has a very small intensity in the FT which could be interpreted due to noise, but with the knowledge of the Raman results it can be decided whether this intensity is physically meaningful or not. Yet, clearly when nitrate groups were evidenced by Raman (for the ceric solutions), the EXAFS simulations including the nitrate contribution are quite convincing, despite the uncertainty on the nitrate coordination number. On the other hand, only free solvated nitrate ions were revealed for the cerous solution by Raman spectroscopy, and the EXAFS simulation with a nitrate contribution appears artificial for the same order of uncertainty on the nitrate number.

4. Conclusions

The reduction of Ce^{4+} to Ce^{3+} in ethanolic solution was studied simultaneously with the combination of time-resolved

X-ray absorption spectroscopy (Quick-EXAFS) at the Ce L_3-edge, UV−vis, and Raman-spectroscopy. A sophisticated in situ cell for the parallel acquisition of all three spectroscopies and a cam-driven, vibrating double-crystal monochromator were employed for the experiments. The results show that high-quality EXAFS-spectra can be obtained on time scales of about 5 s even by using the synchrotron radiation emitted by a bending magnet of a first generation synchrotron radiation source, thus enabling in-depth insights into the mechanisms of the investigated chemical reaction. In the present case, the detailed analysis of the three spectroscopies shows that the Ce^{4+}-content decreases to below ca. 8−9% in about 1800 s, indicating that the local environment around the absorbing Ce-atom has dramatically changed with time, while Ce^{4+} is initially coordinated with two bidentate nitrate and one ethanol; these ligands are released into the solution in the course of the reaction, and our study suggests that the coordination sphere of the remaining trivalent cerium species is only made of water molecules. For the future, the application of combined studies with the above-mentioned techniques on different scientific problems in materials science, such as heterogeneous catalysis, solid-state synthesis, and battery materials, is planned. Moreover, additional techniques such as differential scanning calorimetry (DSC) providing, for example, thermodynamic properties of the materials under investigation will be combined with time-resolved EXAFS measurements.

Acknowledgment. We wish to thank Prof. B. Capelle of Laboratoire de Minéralogie Cristallographie de Paris for the white beam access at the D25 beamline. We would like to thank engineering staff members F. Alves and S. Chagnot of LURE for their manifold technical help during the installation of the Quick-scanning EXAFS monochromator at the DCI storage ring in December of 2003. We would like to thank C. Ringpfeil for help at the beamline during the experiments. Financial support by the MWF Nordrhein-Westfalen, LURE, and Synchrotron SOLEIL is gratefully acknowledged.

References and Notes

(1) Chu, B.; Hsiao, B. S. *Chem. Rev.* **2001**, *101*, 1727−1761 and references herein.

(2) Bras, W.; Ryan, A. J. *J. Mol. Struct.* **1996**, *383*, 309−314.

(3) Everall, H.; Owen, H.; Slater, J. *J. Appl. Spectrosc.* **1995**, *49*, 610−615.

(4) Tashiro, K.; Sasaki, S. *Polym. Sci. Polym. Phys. Ed.* **2002**, *40*, 451−519 and references herein.

(5) Bryant, G. K.; Gleeson, H. F.; Ryan, A. J.; Fairclough, J. P. A.; Bogg, D.; Goosens, J. G. P.; Bras, W. *Rev. Sci. Instrum.* **1998**, *69*, 2114−2117.

(6) Chung, H.; Caffrey, M. *Biophys. J.* **1992**, *63*, 438−447.

(7) Bras, W.; Derbyshire, G. E.; Devine, A.; Clark, S. M.; Cooke, J.; Komanschek, B. E.; Ryan, A. J. *J. Appl. Crystallogr.* **1995**, *28*, 26−32.

(8) Keller, G.; Lavigne, F.; Forte, L.; Andrieux, K.; Dahim, M.; Loisel, C.; Ollivon, M.; Bougaux, C.; Lesieur, P. *J. Therm. Anal.* **1998**, *51*, 783−791.

(9) Jenkins, P. J.; Donald, A. M. D. *Carbohydr. Res.* **1998**, *308*, 133−147.

(10) Bras, W.; Derbyshire, G. E.; Bogg, D.; Cooke, J.; Elwell, M. J.; Komanschek, B. U.; Naylor, S.; Ryan, A. J. *Science* **1995**, *267*, 996−999.

(11) Epple, M.; Sazama, U.; Reller, A.; Hilbrandt, N.; Martin, M.; Tröger, L. *Chem. Commun.* **1996**, 1755−1756.

(12) Tröger, L.; Hilbrandt, N.; Epple, M. *Synchrotron Radiat. News* **1997**, *10*, 11−17.

(13) Wilkin, O. M.; Young, N. A. *J. Synchrotron Radiat.* **1999**, *6*, 204−206.

(14) Tromp, M.; Sietsma, J. R. A.; van Bokhoven, J. A.; van Strijdonck, G. P. F.; van Haaren, R. J.; van der Eerden, A. M. J.; van Leeuwen, P. W. N. M.; Koningsberger, D. *Chem. Commun.* **2003**, *1*, 128−129.

(15) Briois, V.; Belin, S.; Villain, F.; Bouamrane, F.; Lucas, H.; Lescouëzec, R.; Julve, M.; Verdaguer, M.; Tokumoto, M. S.; Santilli, C. V.; Pulcinelli, S. H.; Carrier, X.; Krafft, J. M.; Jubin, C.; Che, M. *Phys. Scr.* **2004**, in print.

(16) Frahm, R. *Nucl. Instrum. Methods* **1988**, *A270*, 578−581.

(17) Fontaine, A.; Dartyge, E.; Itie, J. P.; Polian, A.; Tolentino, H.; Tourillon, G. *Topics in Current Chemistry*; Berlin: Springer, 1989; Vol. 151, pp 180−203.

(18) Richwin, M. Ph.D. dissertation, Universität Wuppertal, 2003 (in german).

(19) Frahm, R.; Richwin, M.; Lützenkirchen-Hecht, D. *Phys. Scr.* **2004**, in print.

(20) Lützenkirchen-Hecht, D.; Grunwaldt, J.-D.; Richwin, M.; Grieseböck, B.; Baiker, A.; Frahm, R. *Phys. Scr.* **2004**, in print.

(21) Doyle, M. P. *J. Chem. Educ.* **1974**, *51*, 131−132.

(22) Prieto, C.; Lagarde, P.; Dexpert, H.; Briois, V.; Villain, F.; Verdaguer, M. *Meas. Sci. Technol.* **1992**, *3*, 325−329.

(23) Newville, M.; Livins, P.; Yacoby, Y.; Stern, E. A.; Rehr, J. J. *Phys. Rev. B* **1993**, *47*, 14126−14131.

(24) Newville, M.; Ravel, B.; Haskel, D.; Rehr, J. J.; Stern, E. A.; Yacoby, Y. *Physica B* **1995**, *208 & 209*, 154−155.

(25) Ankudinov, A. L.; Ravel, B.; Rehr, J. J.; Conradson, S. D. *Phys. Rev. B* **1998**, *58*, 7565−7576.

(26) Beineke, T. A.; Delgaudio, J. *Inorg. Chem.* **1968**, *7*, 715−721.

(27) Zalkin, A.; Forrester, J. D.; Templeton, D. H. *J. Chem. Phys.* **1963**, *39*, 2881−2891.

(28) Fonda, E.; Andreatta, D.; Colavita, P. E.; Vlaic, G. *J. Synchrotron Radiat.* **1999**, *6*, 34−42.

(29) Jackson, J. E. *A user's guide to principal components*; John Wiley & Sons: New York, 1991.

(30) Malinowski, E. R.; Howery, D. G. *Factor analysis in chemistry*; John Wiley & Sons: New York, 1980.

(31) van Lier, J.; Baretzki, B.; Zalar, A.; Mittemeijer, E. J. *Surf. Interface Anal.* **2000**, *30*, 124−129.

(32) Wasserman, S. R. *J. Phys. IV (France)* **1997**, *7*, C2-203−205.

(33) Ressler, T. *J. Synchrotron Radiat.* **1998**, *5*, 118−122. See also: www.winxas.de.

(34) Ressler, T.; Wong, J.; Roos, J.; Smith, I. L. *Environ. Sci. Technol.* **2000**, *34*, 950−958.

(35) Alia, J. M. Ion−ion interactions in electrolyte solutions. In *Handbook of Raman Spectroscopy*; Lewis, I. A., Edwards, H. G. M., Eds.; Marcel Dekker: New York, 2001; pp 617−682.

(36) Karraker, D. G. *Inorg. Nucl. Chem. Lett.* **1968**, *4*, 309−313.

(37) Larsen, R. D.; Brown, G. H. *J. Phys. Chem.* **1964**, *68*, 3060−3062.

(38) Young, B. L.; Trahanovsky, W. S. *J. Am. Chem. Soc.* **1969**, *91*, 5060−5067.

(39) Briois, V.; Williams, C. E.; Dexpert, H.; Villain, F.; Cabane, B.; Deneuve, F.; Magnier, C. *J. Mater. Sci.* **1993**, *28*, 5019−5031.